# Tangential phase-contrast imaging for fluctuation measurements in JT–60SA: a conceptual study

S. Coda[1], A. Iantchenko[1], K. Tanaka[2], S. Brunner[1]

[1] *Ecole Polytechnique Fédérale de Lausanne, Swiss Plasma Center (EPFL–SPC), 1015 Lausanne, Switzerland*

[2] *National Institute for Fusion Science, Toki, Japan*

The new JT–60SA tokamak [1], which is scheduled to begin operating in 2020, presents unique opportunities to advance the physics knowledge base for ITER and DEMO in a truly reactor-grade environment. In particular, fundamental studies of plasma turbulence and of its relation to transport can aid in the understanding and control of foreseeable reactor operational regimes, and potentially guide the way to improving them or discovering new ones. This contribution reports on a feasibility study and preliminary design of a fluctuation diagnostic based on the phase-contrast imaging (PCI) technique, which is being proposed for JT–60SA. It will be shown that this diagnostic will be able to resolve fluctuations as low as $\tilde{n}/n \sim 10^{-5}$ for wave numbers ranging from $k\rho_i \sim 0.06$ to 12 (where $\rho_i$ is the ion sound gyroradius), thus spanning a multiscale range of transport-relevant modes, from ITG to TEM to ETG. A spatial resolution of 5% of the minor radius or less is achieved near the magnetic axis and in the edge region, and of 25% at mid-radius, at $k = 4$ cm$^{-1}$; the resolution improves with increasing $k$.

Phase-contrast imaging [2] is a powerful laser-based technique for imaging line-integrated density fluctuations in plasmas in the plane perpendicular to the laser beam. At each location along the beam path, the measurement selects wave vectors that are perpendicular to both the magnetic field (since turbulence is known to possess a vanishing parallel wave number) and to the beam direction (because of the line integration). This property can be used to achieve some degree of localization by selecting the measured wave-vector direction using, e.g., a spatial filter. In the case of tangential propagation, the achievable localization can be very good, as has been shown on TCV [3]. This is the configuration being proposed for JT–60SA. Optimum resolution is achieved at the point closest to tangency, where the wave-vector direction varies most rapidly, and near the magnetic axis, where the derivative of the flux coordinate with respect to the linear coordinate along the beam path vanishes.

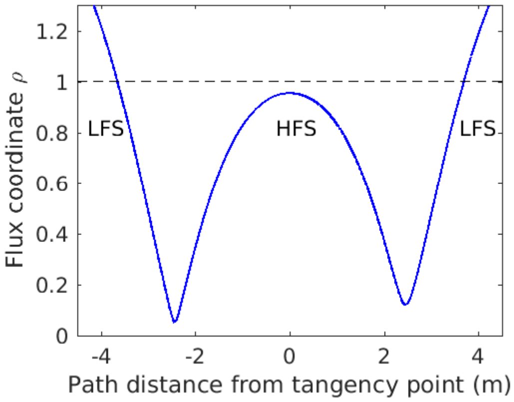

Figure 1: Mapping of PCI beam path to radial flux coordinate (square root of the normalized poloidal flux) for scenario 1.

The geometry being proposed would use two dedicated ports for beam entry and exit, located on the tangential port assemblies P8 and P1 at slightly different vertical positions. The resulting optical path is illustrated in Fig. 1 for the reference scenario 1, a double-null-diverted plasma at full current with 41 MW heating. The tangency point is just inside the last closed flux surface (LCFS) on the high-field side (HFS) and the beam passes also very close to the magnetic axis.

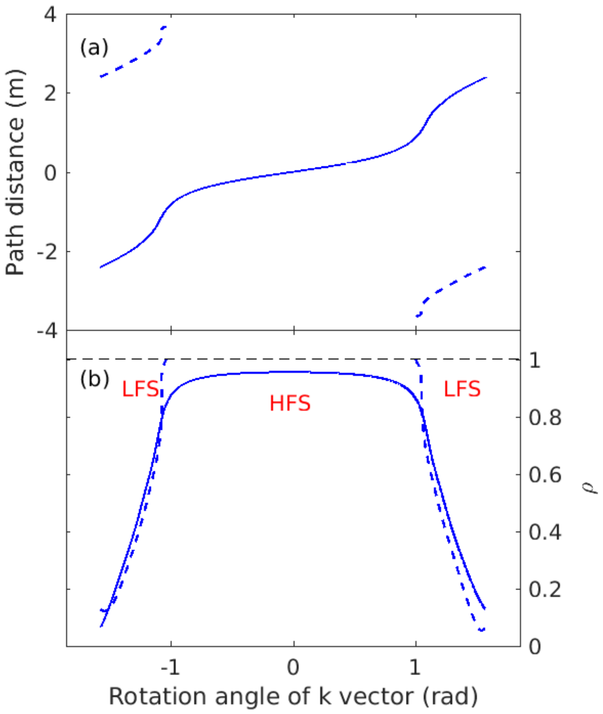

Figure 2: (a) Linear distance from the tangency point and (b) flux coordinate, vs the rotation angle of the wave vector with respect to a horizontal axis, for $k = 4$ cm$^{-1}$ in scenario 1.

The linear coordinate along the beam vs the wave-vector direction (parametrized by an angle in the plane perpendicular to the beam) is partly double-valued, as shown in Fig. 2(a). In the double-valued ranges, the two locations (distinguished by the line type, solid versus dashed) are separated by a significant distance $L$, of the order of 4 m. The addition of these segments of lengths $L_1$ and $L_2$ introduces a non-uniform – but precisely known – transfer function in $k$-space, $T(k) = L_1 + L_2 \cos[k^2 L/(2k_0)]$, $k_0$ being the laser wave number [4]. For $k \gtrsim 5.4$ cm$^{-1}$, PCI loses its strict imaging properties and a deconvolution becomes necessary to recover the image in these spatial ranges. In spite of this complication, in the specific geometry being proposed for JT–60SA the two segments in each double-valued case are invariably closely aligned in $\rho$, as seen in Fig. 2(b). The double-valuedness thus has little impact on the radial localization. The aggregate localization is visualised in Fig. 3.

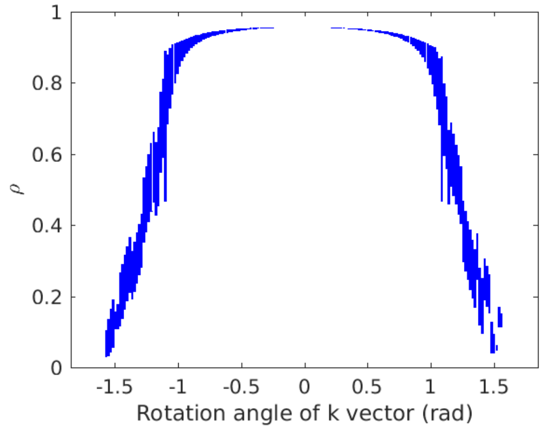

Figure 3: PCI measurement location, depicted as vertical bars including radial spread from diffraction as well as from double segments where relevant, for $k = 4$ cm$^{-1}$ in scenario 1.

The best resolution is nevertheless obtained in the single-valued region near the HFS LCFS. Note that, in terms of $\rho$, there are *two* double-segment measurements for each $\rho$ for a large fraction of the plasma. This is seen explicitly in Fig, 4, which displays the aggregate resolution for varying wave number. As the effect of diffraction decreases with increasing $k$, the filter selectivity improves and the resolution also improves.

The orientation of the measured wave vectors is primarily radial near the axis and at the HFS edge, whereas it is primarily poloidal in the double-segment, mixed HFS-LFS edge measurements. In the latter location it may be possible to separate the HFS and LFS empirically in frequency space through opposite Doppler shifts due to $\mathbf{E}\times\mathbf{B}$ drifts oriented in opposite directions. The wave-number range depends on beam size and detector geometry and is expected to be $0.3 < k < 20\ \mathrm{cm}^{-1}$, which – with a frequency bandwidth of $\sim$1 MHz – would comfortably capture the main ITG and TEM modes expected to contribute the most to transport, in addition to zonal flows and bursty phenomena such as avalanches. A faster detector ($\sim$10 MHz) would also provide access to ETG modes.

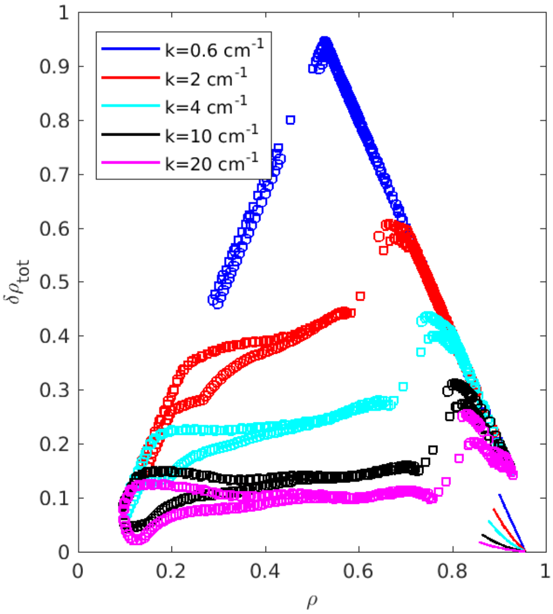

Figure 4: Aggregate radial resolution (solid lines: single-segment regions; symbols: double-segment regions) vs radial coordinate for different wave-number values, for scenario 1.

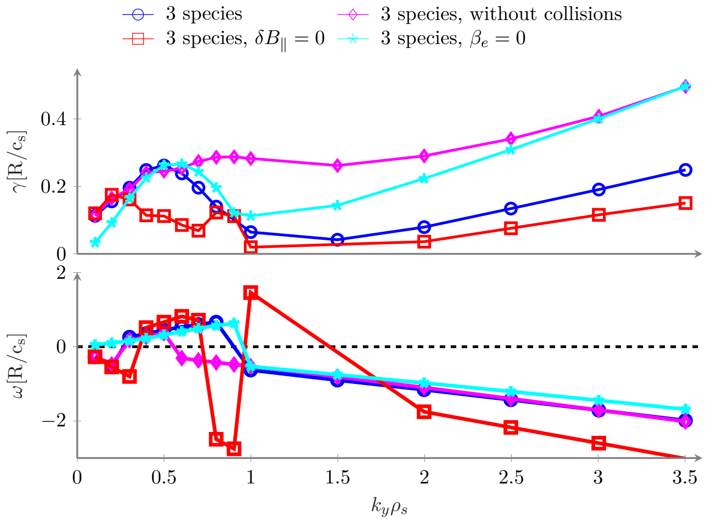

Figure 5: Linear simulation of the most unstable mode's growth rate and frequency vs binormal wave number $k_y$, for three species (main ions, electrons, and carbon impurity ions). The full simulation (blue circles) is compared with a case without collisions (purple diamonds), without parallel magnetic-field fluctuations (red squares), and completely without electromagnetic effects (cyan stars).

The sensitivity of the diagnostic is limited by detector noise and improves with laser power. Phase sensitivity in the $\mu$rad range, corresponding to a line-integrated density below $10^{14}\ \mathrm{m}^{-2}$, can be attained in principle. Depending on the effective integration length, the resulting minimum measurable relative density fluctuation can reach $10^{-5}$.

Eventual measurements on JT–60SA are planned to be supported by and compared to numerical simulations using gyrokinetic codes. In preparation for this and to validate the appropriateness of the PCI design choices, we have performed initial simulations using the GENE code [5] and a synthetic PCI diagnostic. The latter is only preliminary in that it does not yet treat the double segments, rather it models each segment individually. Both linear and nonlinear local (flux-tube) simulations were carried out for the mid-radius region ($\rho \sim 0.5$). The growth rate and frequency of the most unstable linear mode are plotted in Fig. 5 and compared to the results obtained with a variety of approximations commonly used to reduce computational time in the nonlinear case. These modes can generally be identified as a combination of ITG and TEM (positive and negative frequency, respectively). It is clear from this that electromagnetic effects are important for the scenario under study. Fully electromagnetic nonlinear simulations would therefore be appropriate. With the limited resources available for the present study, only an electrostatic flux-tube simulation was carried to steady state in a statistical sense. However, an initial, not yet stationary electromagnetic simulation confirms qualitatively that electromagnetic effects are important in the nonlinear state as well. The final results of the nonlinear electrostatic simulation after processing by the synthetic diagnostic are shown as frequency and wave-number spectra in Fig. 6 for the LFS and HFS of the $\rho \sim 0.5$ flux surface. This confirms that the range of the planned diagnostic is appropriate for resolving the most unstable modes.

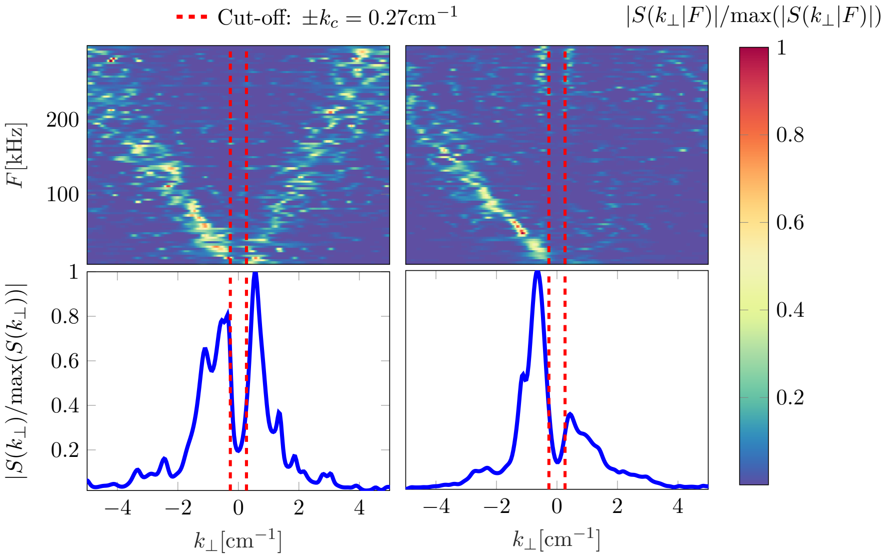

Figure 6: Normalised conditional wave-number and frequency spectra (top), and normalised wave-number spectra (bottom) for the electrostatic simulation, at $\rho$=0.5 on the LFS (left) and HFS (right). Red dashed lines indicate the lowest measurable wave number.

This work has been carried out within the framework of the EUROfusion Consortium and has received funding from the Euratom research and training programme 2014–2018 and 2019–2020 under grant agreement No 633053. The views and opinions expressed herein do not necessarily reflect those of the European Commission. This work was supported in part by the Swiss National Science Foundation.

## References

[1] H. Shirai, P. Barabaschi, and Y. Kamada, Nuclear Fusion **57**, 102002 (2017).
[2] H. Weisen, Review of Scientific Instruments **59**, 1544 (1988).
[3] A. Marinoni, S. Coda, R. Chavan, and G. Pochon, Review of Scientific Instruments **77**, 10E929 (2006).
[4] S. Coda, Ph.D. Thesis, MIT Plasma Science and Fusion Center (1997).
[5] F. Jenko, W. Dorland, M. Kotschenreuther, and B. N. Rogers, Physics of Plasmas **7**, 1904 (2000).